Received: 7 May 2024 | Revised: 3 July 2024 | Accepted: 8 July 2024

DOI: 10.1002/pc.28814

RESEARCH ARTICLE

Polymer COMPOSITES WILEY

A facile approach for enhancing mechanical resilience, and corrosion protection in epoxy coatings using bismuthene nanosheets

Qingshi Meng[1] | Shuangshan Li[1] | Fuyuan Guo[1] | Murat Demiral[2] | Sensen Han[1] | Fanze Meng[1] | Yanxi Zhang[3] | Sherif Araby[4]

[1]College of Aerospace Engineering, Shenyang Aerospace University, Shenyang, China

[2]College of Engineering and Technology, American University of the Middle East, Kuwait, Kuwait

[3]School of International Education, Shenyang Aerospace University, Shenyang, China

[4]Department of Mechanical and Aerospace Engineering, School of Engineering and Digital Sciences, Nazarbayev University, Astana, Kazakhstan

Correspondence

Sensen Han, College of Aerospace Engineering, Shenyang Aerospace University, Shenyang 110136, China.
Email: sausshan@outlook.com

Sherif Araby, Department of Mechanical and Aerospace Engineering, School of Engineering and Digital Sciences, Nazarbayev University, Astana 010000, Kazakhstan.
Email: sherif.gouda@nu.eud.kz

Funding information

National Natural Science Foundation of China, Grant/Award Numbers: 52173077, 51973123; Liaoning Provincial Department of Education Series Project, Australia, Grant/Award Number: LJKZ0187; Natural Science Foundation of Liaoning Province, Grant/Award Number: 2023-MS-239; Liaoning BaiQianWan Talents Program, China, Grant/Award Number: 2021921081; Nazarbayev University, Collaborative Research, Grant/Award Number: 20122022CRP1613

Abstract

This study presents novel mechanochemical methods for the synthesis and chemical modification of bismuthene nanosheets (BINS) using a high-speed blender and planetary ball milling. Atomic force microscopy (AFM) measurements confirmed successful exfoliation of 1.5-nm BINS. Epoxy/BINS nanocomposites exhibited enhanced mechanical properties, thermal stability, and chemical resistance. Chemical modification via ball milling improved the interface and dispersion of BINS within the epoxy matrix, leading to significant enhancements in mechanical performance and chemical resistance. Compared to neat epoxy, at 0.75 vol% m-BINS, Young's modulus, impact strength and fracture toughness K_{IC} were respectively enhanced by 30%, 88.6%, and 144.4% while these increments were 10%, 55.7%, and 97.8% for pristine BINS-based epoxy nanocomposite. A 3D finite element model of the impact test of the nanocomposite was developed to predict its behavior under high-strain rate loadings; the numerical model showed high agreement with experimental measurements. Epoxy/m-BINS nanocomposites demonstrated exceptional chemical resistance, attributed to the small lateral dimensions of m-BINS, which fill the spaces between cross-linked epoxy molecules and uniformly distribute within the matrix. These findings highlight the crucial role of interface and dispersion in defining the mechanical properties of nanocomposites. Overall, this study provides a facile and scalable method for synthesizing and modifying bismuthene, showcasing its potential for developing functional polymer nanocomposites.

Highlights

- Bismuthene nanosheets & modified BINS (m-BINS) are prepared by eco-friendly method.
- m-BINS is ~1.5 nm thick and ~0.5 μm wide.
- m-BINS shows good dispersion and strong interface adhesion within epoxy matrix.

- Impact strength and K_{IC} of epoxy/m-BINS nanocomposite are enhanced by 88.6% and 144.4%.
- Numerical model for impact strength is developed to predict behavior at high-strain rate.

KEYWORDS

bismuthene, functional coating, mechanical property, mechanochemistry, nanocomposite

1 | INTRODUCTION

Graphene,[1,2] MXene,[3,4] hexagonal boron nitride,[5–7] α-ZrP nanosheets,[8–10] and many other 2D materials have attracted significant attention from the scientists for various applications owing to their unique features and advantages depending on its bulk counterparts. For example, graphene and its derivatives[11–13] (graphene oxide, reduced graphene oxide, and graphene platelets) feature superb thermal and electrical conductivity and remarkable mechanical strength where they are employed not only in reinforcing polymers but also for developing thermally and electrically conductive polymers for various applications.[14–17] The plate-like structure of the 2D materials make them unique among other geometries specifically nanotubes or nanorods[18]; plate like structure at the nanoscale offers the most utilized contact surface area with the host matrix provided that complete exfoliation with uniform distribution is attained. Despite significant advancements in nanocomposite materials, there remains a need for novel synthesis methods and effective modification strategies to enhance their mechanical, thermal, and chemical properties.

Bismuthene is an emerging 2D material,[19] consisting of monolayer or few-nanosheets of bismuth. It features high carrier mobility, outstanding specific surface area, high in-plane anisotropy, and buckled honeycomb 2D structure with large lattice constant of 4.357 Å.[20] Compared with other 2D materials in groups IVA and VA, bismuthene has low toxicity, high biocompatibility, and chemical and air stability. This makes bismuthene environmentally friendly and hence attracts researchers to explore its use in various applications, such as catalyst for CO_2 capturing and N_2 fixation.[21]

Mechanochemical method is one of the top–down approach to exfoliate bismuthene nanosheets (BINS) where mechanical forces are used to break van der Waal forces and separate individual nanosheets from a bulk bismuth.[22] The delamination of bismuth layers into BINS is accomplished by mechanical grinding, milling or shearing. A high-speed blender has been employed recently to prepare BINS with high yield; it applies high shear forces with immense turbulence that can facilitate the exfoliation process of a plate-like materials,[23,24] such as bismuth, Ti_3AlC_2 (MAX),[25] and graphite.[26]

Incorporating BINS into polymer matrices is anticipated to open new opportunities for a diverse range of advanced materials and applications, such as flexible and resilient electronics, flexible gas sensors, and biomedical devices. Although bismuthene features unique physical, chemical, and mechanical properties, there is scarcity to find reports or studies on its polymer composites where mechanical and/or chemical properties are investigated. To the best of our knowledge, there is no reports on bismuthine/thermoset nanocomposites. In the current study, we provide a green approach to synthesis and chemically modify BINS. They are exfoliated and modified via a mechanochemical method in two steps. Initially, bismuth powder undergoes exfoliation process using a high-speed blender to produce BINS. Subsequently, a planetary ball-milling is employed to modify BINS with Jeffamine D-400 (they are so-called modified BINS (m-BINS)) to hinder their restacking within the host matrix. Finally, epoxy composites were prepared by incorporating BINS and m-BINS separately. The BINS and its epoxy nanocomposites are thoroughly characterized, and their structure–property relations are extensively investigated including a numerical analysis. The study gives insights into a sustainable production of functional polymer/bismuthene nanocomposites for various applications.

This study aims to synthesize and chemically modify BINS using novel mechanochemical methods, namely a high-speed blender and planetary ball milling, and investigate their effects on the mechanical, thermal, and chemical properties of epoxy nanocomposites. The objective is to enhance our understanding of the role of interface and dispersion in defining the properties of nanocomposites, and to develop a scalable method for the synthesis and modification of BINS for use in functional polymer nanocomposites. This work contributes to the field by providing insights into the design and development of advanced materials with improved performance characteristics. More importantly, this research distinguishes itself by investigating novel mechanochemical methods for synthesizing and modifying BINS,

leading to significant enhancements in mechanical properties and chemical resistance of epoxy nanocomposites, while also developing a validated numerical model for high-speed impact loading.

2 | EXPERIMENTAL AND NUMERICAL MODELING DETAILS

2.1 | Materials

Bismuth powder (200 mesh) was purchased from Anhui Zesheng Technology Co. Ltd. Epoxy (E51, diglycidyl ether of bisphenol-A) was ordered from Nantong Xingchen Synthetic Material Co. Ltd. Jeffamine D 230 and Jeffamine D400 were provided from Huntsman Pty Ltd. Ethanol (99% purity) was purchased from the local market.

2.2 | Preparation

Figure 1 illustrates the process for preparing bismuthenes (BINS). 1 g of bismuth powder and 100 mL of ethanol are added to a plastic container. The container is placed on a Vitamix high-speed blender (Model number E310) for 15 min at 25,900 rpm (7th gear). The blending time divided into three 5-minute intervals; after each interval, the blender is allowed to cool down for 10 min. Once the blending is complete, the resulting suspension is transferred to a plastic tube and centrifuged for 15 min at 3000 rpm. The tube is then dried in an oven at 60°C for 2 h. The dried product is BINS. It noteworthy to mention that the yield is 30%; 0.3 g of BINS for every 1 g of bismuth powder.

The process of modifying bismuthenes (BINS) with Jeff-amine D-400 (D400) is depicted in Figure 1. BINS are combined with D400 in a stainless-steel pot at a weight ratio of 1:1. The mixture is then ball-milled using stainless-steel balls of various sizes at a weight ratio of 50:1 to the BINS and D400 mixture. The planetary ball-milling process is performed for 6 h at 400 rpm, with 10-min breaks every 30 min to prevent overheating. The resulting mixture is washed at least twice with 100 mL of ethanol and dried at 60°C for 2 h resulting in m-BINS.

The process for preparing epoxy composites with BINS and m-BINS is also shown in Figure 1. Epoxy resin was prepared using E-51 and Jeffamine D230 (hardener) at ratio of 1:0.33. Predetermined quantity of BINS or m-BINS is added to the epoxy resin, the composite mixture manually stirred for 5 min then magnetically stirred for 10 min. The mixture is degassed in a freeze dryer for 10 min to remove any trapped air bubbles. The mixture is poured into a waxed-PTFE mold for curing. The curing process is conducted in fan oven for 12 h including: (i) 4 h to increase the temperature from 20 to 120°C at rate 25°C/h and (ii) 8 h at constant temperature of 120°C. Epoxy composites with BINS or m-BINS are prepared at fractions 0.25%, 0.5%, 0.75%, and 1%.

2.3 | Characterization

Chemical groups attached to the BINS and m-BINS are studied using a Fourier transform infrared spectroscopy (FTIR) with a Thermo Scientific Nicolet iS50, within the range of 4000–400 cm^{-1}. Thermogravimetric analysis (TGA) was performed using a Shimadzu DTA-50 at the scan rate of 10°C/min, and the fraction of grafted molecules was characterized by weight loss from room temperature to 800°C in N_2 atmosphere.

The grafting percentage (G_p) can be calculated using the following formula:

$$G_p = \frac{W_a - W_b}{W_a}, \quad (1)$$

where W_a is the weight of the grafted sample after reaction, W_b is the weight of the original sample before

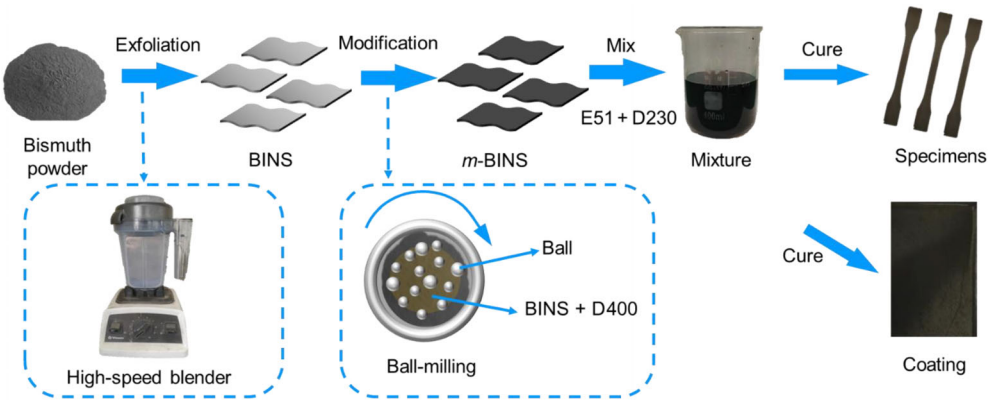

FIGURE 1 Schematics for preparation of bismuthene nanosheets (BINS), modified BINS (m-BINS), and their nanocomposites.

reaction. This formula calculates the percentage increase in weight after grafting, relative to the original weight of the sample before grafting, and expresses it as a percentage.

Atomic force microscopy (AFM) was used to measure the thickness and lateral size of BINS and m-BINS using a Bruker Dimension Icon instrument. The AFM samples were prepared by suspending BINS or m-BINS in acetone at 0.005 wt% via 30 min of sonication and dropping the suspension on mica sheets, followed by drying in a fan oven at 80°C.

Scanning electron microscopy (SEM, ZEISS Sigma 300) was employed to examine the fracture surface of epoxy composites with BINS or m-BINS at 10 kV. X-ray diffraction (XRD) test was conducted epoxy composites using a Rigaku Dmax Ultima+, where Cu Kα radiation was applied at 40 kV and 40 mA. The diffraction patterns were then collected in a reflection mode geometry within 2θ range of 10°–80° at a scanning rate of 10°/min.

Tensile testing was performed on dumb-bell shaped samples at an extension rate of 5 mm/min using a tensile machine (WDW-100E) according to ASTM D-638. The tensile specimens were $170 \times 10 \times 4\ mm^3$, with a gage length of 115 mm. Compact tension (CT) test was carried out using a tensile machine (XIANGMIN), where the K_{IC} and G_{IC} values were calculated according to ISO 13586. The impact strength was carried out on a Charpy impact testing machine (AELTA XJJY-50) with the specimens of dimensions $65 \times 12 \times 4\ mm^3$. Five samples were tested for each nanocomposite fraction for the tensile, CT and impact tests. Dynamic mechanical analysis (DMA) was conducted at a frequency of 1 Hz using a DMA Q800 TA Instrument, Inc., USA. DMA was run using samples of dimensions $35.5 \times 13 \times 3\ mm^3$ within temperature range 25–150°C. Chemical resistance was tested according to ISO 1817-2005.

3 | NUMERICAL MODELING OF IMPACT TEST

A 3D finite element (FE) model of the Charpy impact test was developed in Abaqus software to investigate the contribution of bismuthene on the performance of the neat epoxy. A schematic depiction with some details of the model is shown in Figure 2. To prevent a convergence issue in the solutions, an explicit time integration method was employed in the simulations rather than an implicit one. This allowed for the capture of the workpiece's sudden failure during the test. The workpiece has dimensions of $65 \times 12 \times 4\ mm^3$, in accord with the experiments. Eight-noded linear brick elements with reduced integration and hourglass control were used to describe its behavior. Element size of $0.3 \times 0.3 \times 0.3$ mm was used in the discretization. The mesh convergency was verified by this mesh size since the workpiece's energy absorption ratio to that of the finer mesh ($0.15 \times 0.15 \times 0.15$ mm) was less than 5%. Rigid elements (R3D4) were used to model the striker and stoppers, with a mesh size of $0.4 \times 0.4 \times 0.4$ mm. They were coarser than the workpiece sample with their slave surfaces because, in contact modeling, they were master surfaces. With an impact speed of 3.8 m/s and a mass of 2.077 kg, the impactor generates an impact energy of 15 J. Its surface is plane. The stoppers are fixed in all directions. A general contact algorithm was implemented between the striker-sample and sample-stopper with a friction coefficient of 0.25.[27]

Elasto-plastic with ductile damage model[28] was used to represent the behavior of neat epoxy and epoxy/m-BINS nanocomposite samples. The onset of damage is based on the equivalent plastic strain, i.e. when the strain reaches to a critical value, the damage initiates in the sample. Later, the evolution of the damage is governed by the following energy equation:

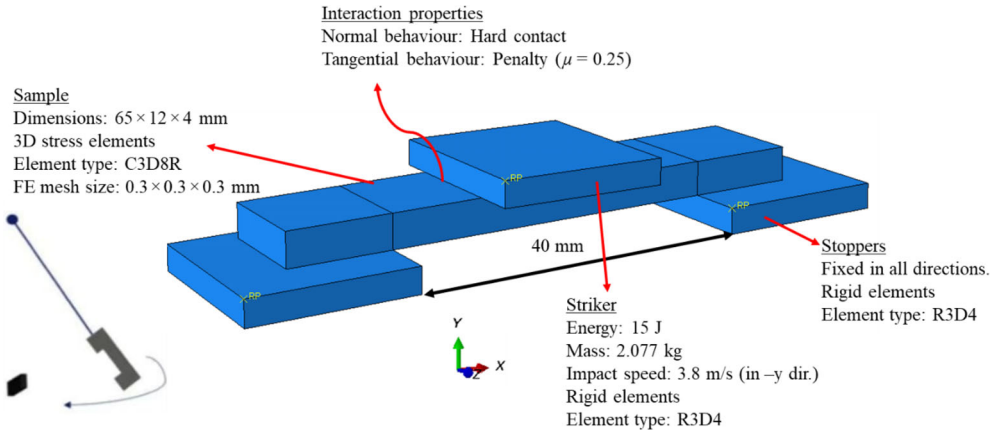

FIGURE 2 Details about the 3D finite element (FE) model of the Charpy impact test.

$\bar{u}_f^{pl} = 2G_f/\sigma_{y0}$, (2) where $\bar{u}_f^{pl}$ is the effective plastic displacement at failure, G_f is the fracture energy per unit area, and σ_{y0} is the yield strength at the time when the failure criterion is reached. The elements in the mesh were deleted upon the complete damage was reached.[29] The material constants obtained from this work and the literature were used (see Table 1).

4 | RESULTS AND DISCUSSIONS

4.1 | Morphology of nanosheets

AFM is employed to measure the thickness of BINS and m-BINS as shown in Figure 3A,B. Figure 3A illustrates an AFM micrograph of bismuthene which has width of ~2 μm and thickness of ~1.5 nm indicating successfulness of high shear blending in exfoliating bismuthene. Figure 3B shows the thickness profile of randomly selected sheet recording thickness of 1.6 nm with width of 0.5 μm. Figure 3C,D shows histograms of thickness and width of m-BINS where the majority of sheets have thickness of ~1.6 nm and width of ~0.4 μm. The AFM results indicate that BINS were successfully exfoliated via mechanochemical method using a high-speed blender. Since the process of modification is performed by high-speed planetary ball milling, BINS can break into smaller lateral dimensions. Also, it is obvious that ball milling develops damages over the BINS surface in the shape of irregular holes as shown in Figure 3C. This is due to the high shear effect and friction between the ball milling spheres and BINS surface. The thickness of m-BINS is larger than pristine BINS due to the attachment of chemical surfactant D400 onto the surface.

FTIR is commonly used to study the functional groups on the surface of nanomaterials after modification.[31,32] Figure 3E shows FTIR spectra of BINS, m-BINS, and D400, illustrating the grafting of D400 molecules onto the surface of BINS. Upon modification, several new peaks emerged: two peaks represent the N—H stretching vibration at 3446 m^{-1} and 1630 cm^{-1}; two peaks assigned to the CH_3 stretching vibration at 2970 m^{-1} and 2873 cm^{-1}; one peak ascribed to the CH_3 flexural vibration at 1373 cm^{-1}; and one peak attributed to the C—O—C stretching vibration at 1106 cm^{-1}. The above grafted chemical groups are from the nucleophilic substitution and ring opening reaction. The FTIR spectra confirm the success of BINS modification with D400 using planetary-ball milling.

TGA was also conducted in order to quantify the grafting ratio of D400 on BINS surface. Figure 3F shows the TGA curves of BINS, m-BINS, and D400. The curves of BINS and m-BINS show a slight weight loss of 0.5% at 100–150°C which is attributed to the evaporation of absorbed water molecules. In the curve of m-BINS, an obvious weight loss is observed in the temperature range of 200–400°C, indicating the pyrolysis of the grafted groups. The grafting ratio was calculated as 3.0% by comparing the weight loss of BINS and m-BINS at 800°C as shown in the inset in Figure 3F.

In Figure 3G, both BINS and m-BINS show the same diffraction peaks as bismuth, except for two negligible oxidation diffraction peaks, and they have similar heights of diffraction peaks. However, m-BINS exhibit a broader diffraction peak at $2\theta = 27.22°$ in Figure 3H. This can be caused by the intercalation of some molecules of D400 into the layers of BINS. The change in diffraction peaks between BINS and m-BINS confirms further the success of modification.

Two epoxy nanocomposites at 0.75 vol% are studied by transmission electron microscopy (TEM), as shown in Figure 4A–D. Figure 4B highlights the presence of thinner BINS, indicated by the yellow arrow, while a significant number of BINS aggregates, marked by red arrows, can be observed. This signifies inadequate dispersion of BINS within the epoxy matrix. Conversely, in Figure 4C, m-BINS are uniformly dispersed throughout the entire matrix. Abundant m-BINS, indicated by the yellow arrow, are visible, with minimal aggregation. This indicates excellent dispersion of m-BINS within the epoxy matrix. Furthermore, these nanosheets exhibit thinner thickness and smaller width, facilitating a superior interface with the epoxy matrix. This enhanced interface contributes to the improved performance of various properties in the composite material.

XRD was also used to investigate the microstructure of epoxy/BINS and epoxy/m-BINS composites. Figure 4E,F shows the XRD patterns of neat epoxy, BINS, m-BINS, and their 0.75 vol% nanocomposite. In Figure 4E, neat epoxy shows a wide diffraction peak from 10° to 30°,

TABLE 1 Constants of neat epoxy and epoxy/m-BINS (0.75 vol%) used in FE analysis.

Sample	Elastic modulus, E (GPa)	Poisson's ratio, υ	Critical equivalent plastic strain (Onset of damage)[30]	Fracture energy, G_f (J/m^2)
Neat epoxy	1.40	0.33	0.25	0.2
Epoxy/m-BINS (0.75 vol%)	1.83		0.25	0.5

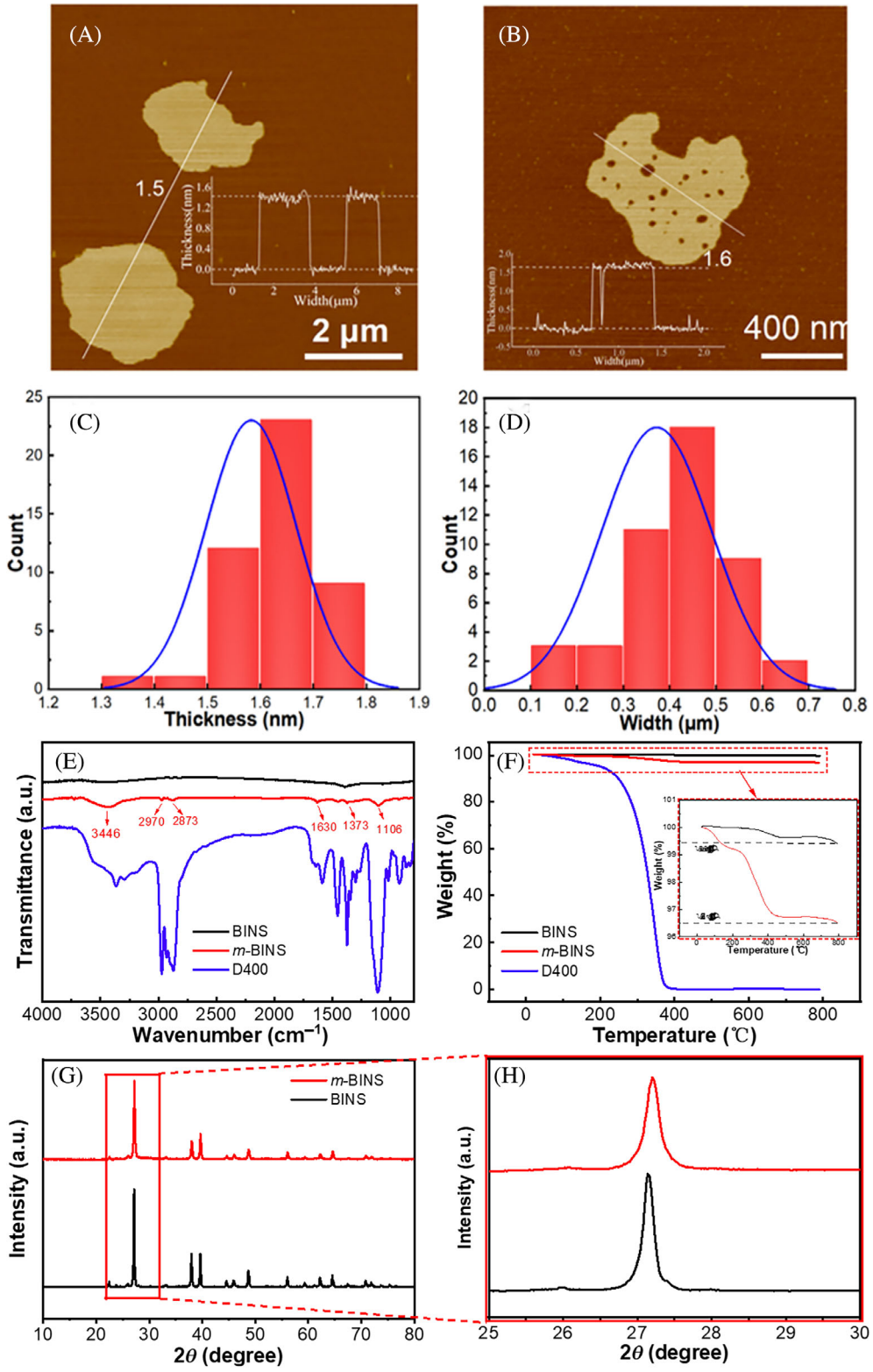

FIGURE 3 Atomic force microscopy image, histogram of thickness and width for (A, C) BINS and (B, D) m-BINS; (E) Fourier transform infrared spectra of BINS, m-BINS, and D400; (F) Thermogravimetric analysis curves of BINS, m-BINS, and D400; and (G, H) X-ray diffraction curves of BINS and m-BINS.

which is attributed to the scattering of the cured epoxy molecules; similar results were observed in previous studies.[33] The XRD patterns of epoxy nanocomposites with pristine BINS or m-BINS show same peaks. However, the intensities are much less in the case of m-BINS system. When the peak around $2\theta = 27.22°$ is zoomed in as shown in Figure 4F, it appears that the peak of epoxy/m-BINS nanocomposite is much wider than that of epoxy/BINS system. Quantitively, the peak of each system was analyzed by OriginLab software; the FWH of m-BINS's peak is 1.38 times the FWHM of pristine BINS's peak. Similar measurement was observed of the peak area, the area of

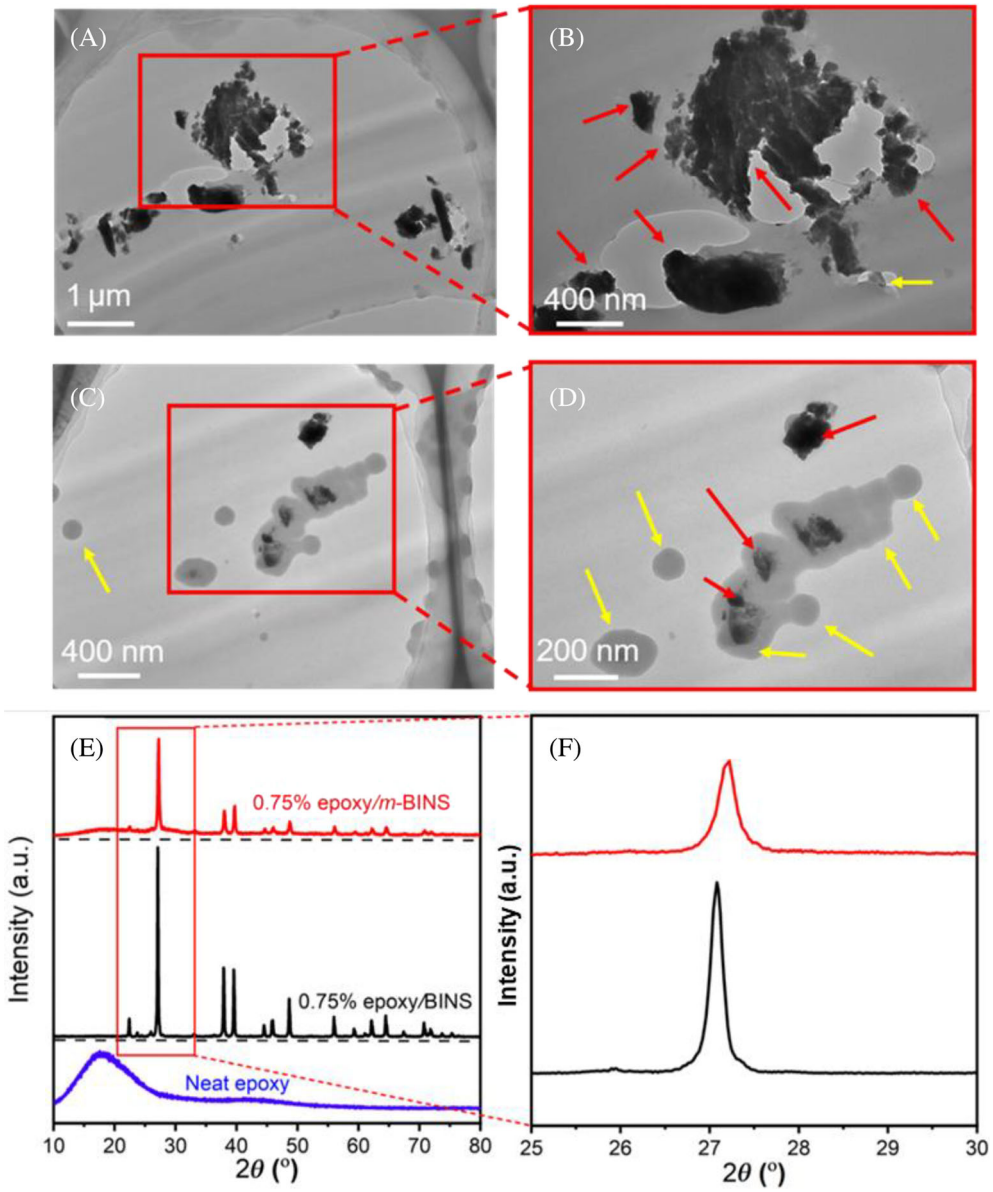

FIGURE 4 (A, B) Transmission electron micrographs (TEM) of the 0.75 vol% epoxy/BINS nanocomposite; (C, D) TEM micrographs of the 0.75 vol% epoxy/m-BINS nanocomposite; and (E, F) X-ray diffraction patterns of neat epoxy and its nanocomposites.

m-BINS's peak was 66% less than of BINS one. Large FWHM and small peak area suggest better dispersion and less BINS filler concentration in the measurement area. This indicates that chemical modification enhances dispersion of BINS within the matrix; similar conclusion was reported in previous studies.[34,35]

4.2 | Mechanical properties

Figure 5A–C shows mechanical properties of neat epoxy and its nanocomposites with pristine BINS and m-BINS. It is evident that BINS have positive impact on the mechanical performance of epoxy. The mechanical properties including tensile strength and impact strength steadily increase with the addition of BINS, in particular at low fractions. Figure 5A compares stress–strain curves of neat epoxy, 0.75 vol% BINS and 0.75 vol% m-BINS nanocomposite. It is evident that pristine BINS-based nanocomposites exhibited brittle rupture, while m-BINS-based nanocomposites showed an early necking behavior which resembles the fracture behavior of neat epoxy reflecting the effect of small lateral dimensions of m-BINS. Remarkably, m-BINS increase the mechanical properties of epoxy in comparison with BINS; at 0.75 vol % of BINS, the tensile strength increases from 62.5 MPa of neat epoxy to 69.6 MPa, representing an 11.4% increment. Meanwhile, at the same content, m-BINS increases the tensile strength of epoxy to 75.4 MPa, showing a 20.6% increment. In a similar fashion, Young's modulus of epoxy marginally increases with the addition of pristine BINS while it has evident increment when m-BINS

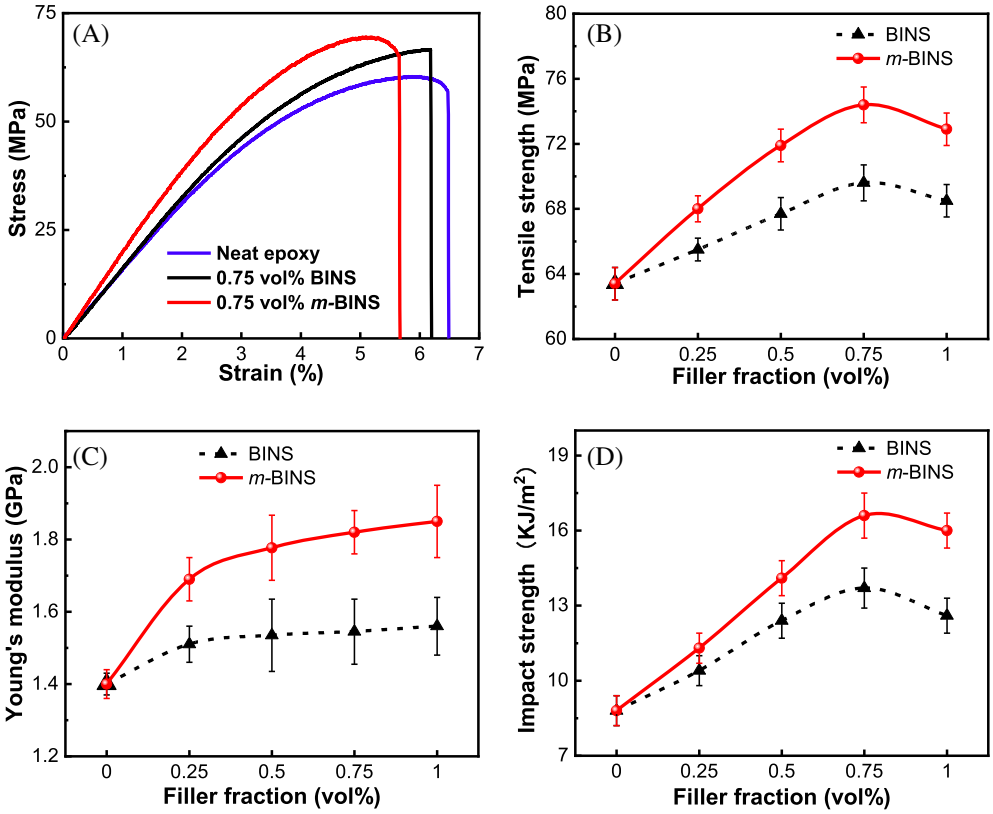

FIGURE 5 Tensile properties of neat epoxy and its bismuthene nanosheets and m-BINS nanocomposites: (A) tensile strength, (B) Young's modulus, (C) stress–strain curves, and (D) impact strength.

is incorporated as shown in Figure 5C. For example, at 0.75 vol%, Young's modulus gained an increment of 30% with m-BINS while this increment was only 10% in case of pristine BINS. However, as the BINS content increases to 1 vol%, the mechanical property either starts to drop like the tensile strength or it has marginal increment as in Young's modulus.

Figure 5D presents the impact strength of neat epoxy and its nanocomposites. The impact strength of both systems shows a significant increase at 0–0.75 vol %, but the enhancement diminishes at 1 vol%. Once again, the effect of chemical modification is highlighted when comparing. The impact strength of epoxy/m-BINS nanocomposites with epoxy/BINS nanocomposites. At 0.75 vol% of pristine BINS, the impact strength increases from 8.8 kJ/m^2 of neat epoxy to 13.7 kJ/m^2, representing a 55.7% increment while this increment is elevated to 89% when m-BINS is added. For epoxy/BINS nanocomposites, the presence of aggregations and clusters of BINS filler particles is evident, which can lead to stress concentration and reduced mechanical properties. In contrast, the epoxy/m-BINS nanocomposites exhibit a more uniform distribution of m-BINS, which can enhance load transfer and improve mechanical properties.

In the light of the obtained results of tensile strength properties and impact strength, it is evident that bismuthene improve the mechanical performance of epoxy. Also, it is evident that chemical modification of BINS with Jeffamine D400 further enhances this performance in comparison with pristine BINS. This can be explained as following: (i) the contrast in mechanical properties of BINS and matrix makes BINS effectively able to reinforce epoxy matrix provided that uniform dispersion is attained. The calculated in-plane stiffness of monolayer bismuthene is 25 N/m[36]; since there is no reports about stiffness of bismuthene in N/m^2, we followed analogy of the published data of graphene's stiffness: graphene's Young's modulus is 330 N/m and 1×10^{12} N/m^2; this will give an approximate of bismuthene's Young's modulus of 76 GPa while the Young's modulus of neat epoxy is within range 1–3 GPa. (ii) Modifying BINS with Jeffamine D-400 surfactant wraps the sheets and prevent them from restacking within the matrix. This increases the contact surface area between BINS and matrix leading to strong interface and effective stress and load transfer between them. Also, the free amine group on D-400 surfactant may covalently bonded with epoxide group in the matrix which can further strengthens the interface with the matrix. On the other hand, pristine BINS did not show similar increments compared with m-BINS mainly because the high chance of restacking and weak interface with the matrix.

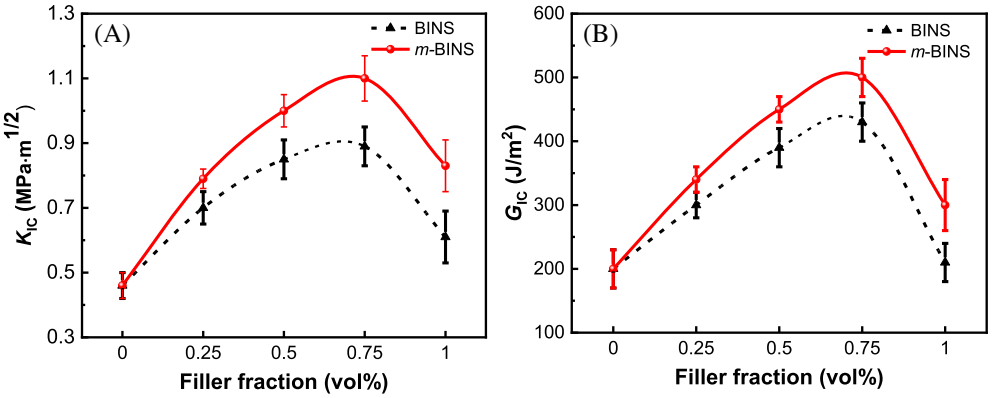

FIGURE 6 Toughness properties of epoxy/bismuthene nanosheets (BINS) and modified BINS (m-BINS) nanocomposites: (A) K_{IC} and (B) G_{IC}.

Figure 6 shows the plane-strain fracture toughness K_{IC} and critical strain energy release rate G_{IC} of neat epoxy and its nanocomposites with BINS and m-BINS. The K_{IC} and G_{IC} of both systems show a significant increase with filler content range 0–0.75 vol% then starts to decrease. Additionally, the K_{IC} and G_{IC} of epoxy/m-BINS nanocomposites are significantly higher than those of epoxy/BINS nanocomposites. At 0.75 vol% of BINS, the K_{IC} increases from 0.45 MPa·m$^{1/2}$ of neat epoxy to 0.89 MPa·m$^{1/2}$, representing a 97.8% increment while it increased by 144.4% when 0.75 vol% of m-BINS is added. Similarly, at 0.75 vol% G_{IC} increases from 206 J/m^2 of neat epoxy to 435 J/m^2 (115% increment) in case of pristine BINS; this increment was 150% upon modifying BINS. However, as the volume fraction of filler increased further, the K_{IC} and G_{IC} began to decrease at 1 vol% due to stress concentration caused by filler aggregation.

The results are explained as follows. Upon modification, m-BINS exhibits a better interface and dispersion in the epoxy matrix since the chemical bond grafted on the m-BINS' surface strengthens the interface with the matrix. This strong interface results in high energy release. Additionally, the incorporation of m-BINS restricts the mobility of the epoxy's chain, resulting in higher stiffness. At low filler fraction (<0.75 vol%), fillers have plenty of space to disperse, enabling them to establish strong interactions with the matrix. Consequently, stress transferring and load sharing between the filler and matrix are significantly improved. However, at high filler fraction, the fillers tend to swarm and aggregate, leading to the formation of clusters. These aggregates can create stress concentration sites where cracks are more likely initiated. As a result, the mechanical properties are negatively affected.

Also, lateral dimensions of nanofiller plays a crucial role in achieving uniform dispersion. Since modifying BINS was via planetary ball milling, they break down into smaller sheets; in case of pristine BINS, they have an average width of ~1.5 μm compared with 0.5 μm of m-BINS. Therefore, the dispersion of m-BINS in the matrix is further improved after modification. Large fillers could form aggregates through overlapping with the adjacent fillers. Excessive overlapping can weaken the stress sharing between the matrix and filler, and act as stress concentration locales. This is another reason why higher increments in mechanical properties occur in epoxy/m-BINS nanocomposites in comparison with pristine BINS system.

The FE simulation of the Charpy impact test was performed. The strain rate during the impact test was approximately 10^3 s^{-1}, as our first FE simulations showed. As a result, the quasi-static yield strength values shown in Figure 6 cannot be used in the simulations. Jung et al.[30] identified the mechanical properties of neat epoxy and carbon nanotube reinforced epoxy composites at high strain rates using Split Hopkinson pressure bar test. This investigation showed that neat epoxy acted like a brittle material with elastic and very limited perfect plastic characteristics at higher strain rates. This study reported that the neat epoxy strength value was 105.90 MPa and the failure strain was 0.40 at a strain rate of 1200 s^{-1}. In contrast, these values were 53.4 MPa and 5.0 when the sample was under a quasi-static loading. In the simulations here, the properties from[30] obtained at high strain rate (very much close to that of impact test), therefore, they were used.

Figure 7A,B demonstrates the deformed shapes of neat epoxy specimen obtained experimentally and numerically with the distribution of onset of damage, where they are observed to be consistent. Figure 7C presents the change in the speed of the striker during the impact test obtained from the simulations. It was observed that upon the contact of the striker to the sample, its speed started to decrease until reaching to 3.7426 m/s at $t = 0.40$ ms. That means the complete failure of the specimen, that is end of the energy absorption of the specimen, occurred at this instant. With the help of this figure, the impact strength of the neat epoxy can

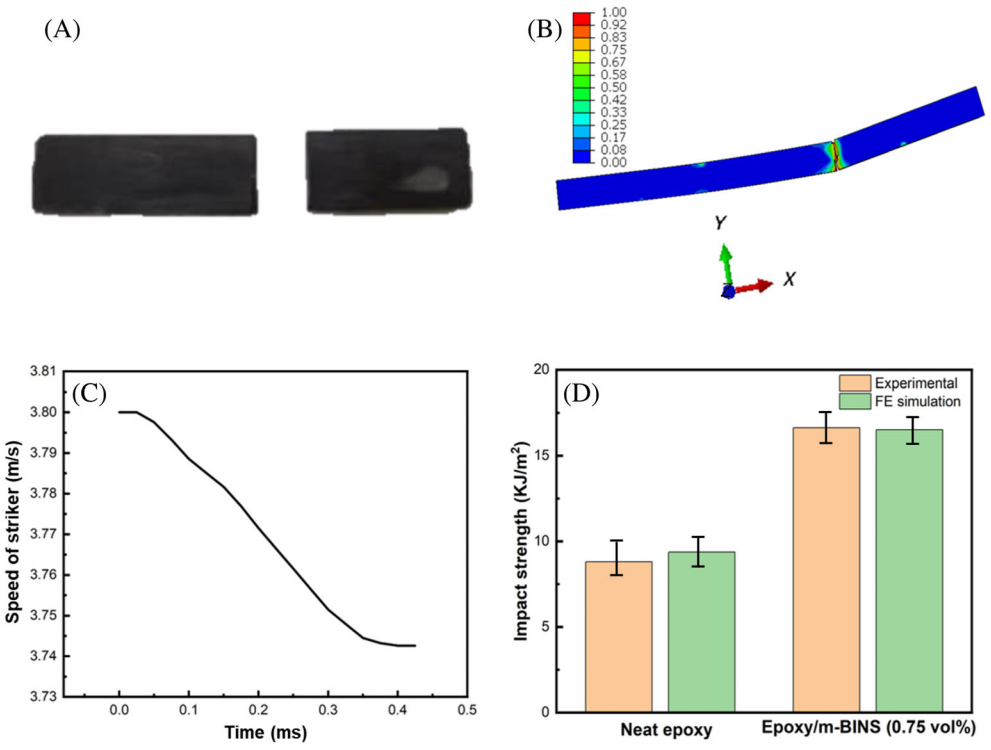

FIGURE 7 Deformed shape of the neat epoxy sample obtained (A) experimentally and (B) numerically; (C) The variation of the speed of the striker with time during the impact test; (D) Impact strength of neat epoxy and its modified bismuthene nanosheets (m-BINS) nanocomposite experimentally and numerically.

be computed as follows: the sample's energy absorption, the striker's kinetic energy decreases during the impact, divided by the area of its cross-section where the failure happened (12 × 4 mm). It was computed to be 9.36 kJ/m^2, which is consistent with the experimentally obtained value, 8.80 kJ/m^2 as shown in Figure 7D.

After verifying the developed FE model, the prediction was performed for epoxy/m-BINS (0.75 vol%) showing the best mechanical performance among all the specimens in the experiments. As the epoxy/m-BINS exhibited better dispersion, compatibility and interface with epoxy matrix compared with epoxy/BINS, its description with the FEs with homogenous material model was expected to be better; therefore, it was considered here. However, its yield strength under high strain rate is not available. For this purpose, 127.75 MPa was considered here (called as Scenario 1, see Table 2) as this number was calculated based on the ratio of yield strength values for the epoxy/m-BINS (0.75 vol%) (53.40 MPa) and neat epoxy (44.30 MPa) obtained in this study. It was assumed that the ratio of their yield strength values obtained quasi-statically here was considered to be identical at higher strength values (127.65 to 105.90 MPa). The respective FE simulation demonstrated that the impact strength value was 13.33 kJ/m^2, around 20% less than the one observed in the experiment in this study, 16.63 kJ/m^2 (see Figure 5D). This result revealed that epoxy/m-BINS (0.75 vol%) behaved much stronger under impact loading, therefore it absorbed excessive amount of energy. Our further FE simulations demonstrated that for the yield strength value of 165.46 MPa (called as Scenario 2), the impact strength was calculated to be 16.51 kJ/m^2, which was in line with the experimentally observed one. This strength value was around 56% larger than that of the neat epoxy, whereas this difference was around 21% for quasi-static loading condition as presented in Table 2. In the simulations, the critical failure strain was considered to be identical for both neat epoxy and nanocomposite (see Table 1). However, with the addition of m-BINS into epoxy, the failure strain was observed to decrease in quasi-static experiments here (see Figure 5A). If this would be the case at higher strain rate, the ratio of the strength of epoxy/m-BINS (0.75 vol%) to neat epoxy would be even larger than 1.56. Overall, it was revealed that with the contribution of m-BINS into epoxy, the increase in the strength of nanocomposite was much larger when it was subjected to higher loading rates in comparison to that subjected to quasi-static loadings.

4.3 | Dynamic mechanical analysis

DMA was conducted to assess the effect of adding BINS into epoxy matrix and evaluate the interface effect on thermal properties of epoxy nanocomposites. DMA is a justified measurement tool to examine the molecular relaxation process and determine the glass transition

TABLE 2 Mechanical properties of neat epoxy and epoxy/m-BINS used in and obtained from finite element analysis.

Neat epoxy			Epoxy/m-BINS (0.75 vol%)		
Yield strength (MPa)[30]	Impact strength (kJ/m^2)		Yield strength (MPa)	Impact strength (kJ/m^2)	Ratio of yield strength of nanocomposite to neat epoxy
105.90	9.36	Scenario 1	127.65	13.33	1.21
		Scenario 2	165.46	16.51	1.56

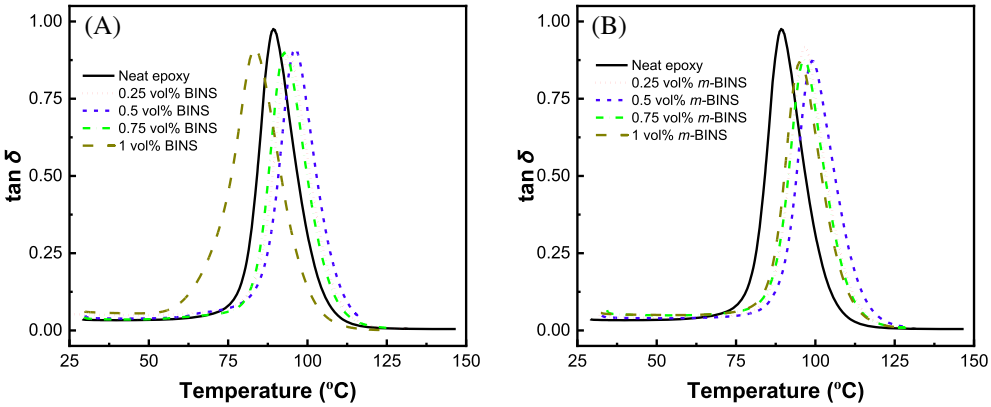

FIGURE 8 Tan delta for (A) epoxy/BINS and (B) epoxy/m-BINS nanocomposites. BINS, bismuthene nanosheets; m-BINS, modified BINS.

TABLE 3 Glass transition temperature of neat epoxy and its nanocomposites.

Filler fraction (vol%)	Glass transition temperature, T_g (°C)	
	Epoxy/BINS	Epoxy/m-BINS
0	89.2	89.2
0.25	94.2	96.7
0.5	95.9	98.9
0.75	92.1	96.5
1	86.3	93.4

temperature (T_g) where the polymeric molecules are rearranged and transferred from glassy state to viscoelastic state. Figure 8A,B presents the tan δ for neat epoxy and its nanocomposites with pristine BINS and m-BINS as a function of temperature. A decrease in tan δ amplitude signifies a significant restriction in matrix chain motion,[34] which is observed in both pristine BINS and m-BINS-based nanocomposites. This is due to the existence of stiff filler, BINS, which restricts the mobility of epoxy at high temperature. Similar behavior was observed in epoxy/graphene nanocomposites.

Table 3 summarizes the T_g values for both neat epoxy and its nanocomposites. Notably, T_g of epoxy increases with the addition of pristine BINS (0–0.75 vol%) or m-BINS (0–1 vol%). However, the increments in T_g values in m-BINS are more pronounced; for example, at 0.5 vol%, T_g increased by 10°C in case of m-BINS while it is 6°C for pristine BINS. The chemical modification effect was more evident at high fraction; pristine BINS showed a decline in the T_g of epoxy by ∼3°C at 1 vol% in comparison with neat epoxy, while it is still higher than the neat epoxy by ∼4°C in case of m-BINS. This is another confirmation that strong interface and uniform dispersion are important and can be attained when chemical modification is employed on BINS before mixing with epoxy. At lower fractions, the improvements in T_g are primarily attributed to two factors: (i) the uniform dispersion of m-BINS, which enhances and strengthens the crosslinking density; and (ii) the strong interface resulting from D-400 molecules bridging BINS with the epoxy matrix. Conversely, T_g reductions at higher filler fractions occur due to filler aggregation.

4.4 | Fractography analysis

SEM was investigate the fracture mechanism of epoxy nanocomposites and to detect any agglomeration or clusters. The SEM images of the fracture surface from tensile testing and CT of neat epoxy are not presented here, as neat epoxy exhibited a smooth, featureless fracture surface.[37] Two specific filler fractions, 0.25 and 0.75 vol% were selected as they represent the beginning and

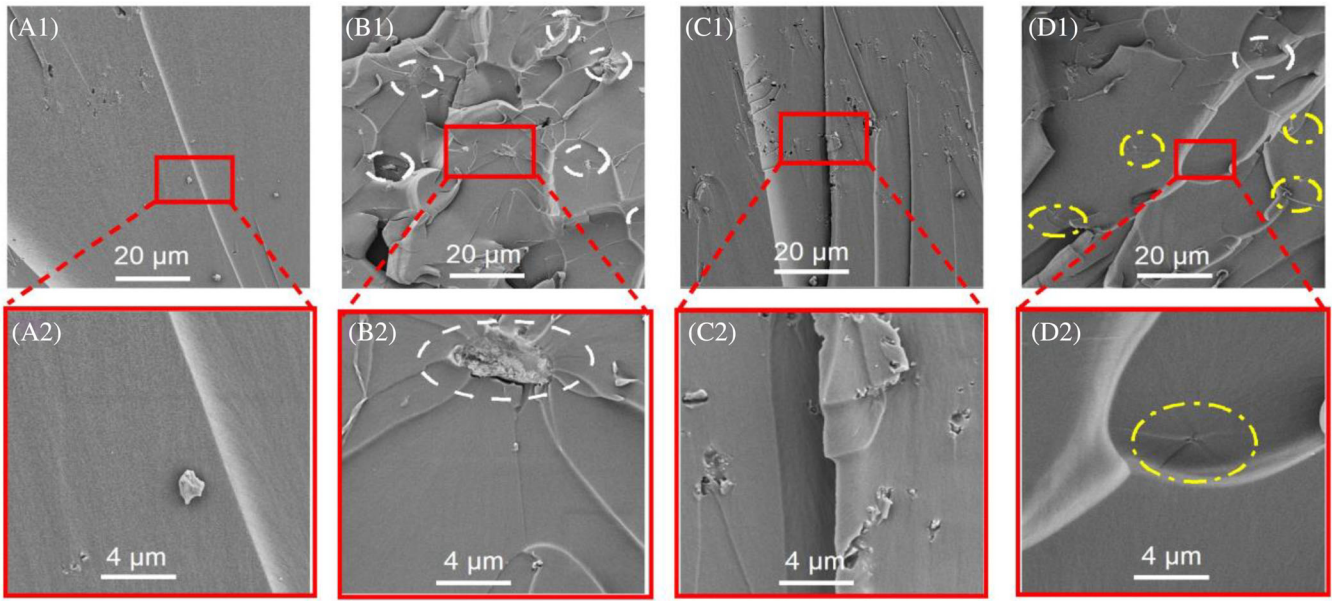

FIGURE 9 Scanning electron microscopy images of fracture surface of tensile testing samples with: (A1, A2) bismuthene nanosheets (BINS) at 0.25 vol%; (B1, B2) BINS at 0.75 vol%; (C1, C2) modified BINS (m-BINS) at 0.25 vol%; and (D1, D2) m-BINS at 0.75 vol%.

maximum reinforcement of mechanical properties, making them valuable for analyzing the strengthening mechanism of BINS and m-BINS in epoxy.

Figure 9 shows the SEM images of fracture surfaces after tensile testing the epoxy/BINS and m-BINS nanocomposites. The SEM image of the 0.25 vol% m-BINS nanocomposite reveals a rougher fracture surface, and the distribution of the energy release area appears more uniform compared with the fracture surface of pristine BINS-based composite. Similarly, the SEM image of the 0.75 vol% m-BINS nanocomposite displays highly rough fracture surface in comparison with the 0.75 vol% BINS nanocomposite. Figure 9B1 displays aggregations of BINS, marked with white circles; Figure 9B2 shows a typical example of an aggregation. On the other hand, the fracture surface of the 0.75 vol% m-BINS nanocomposite shows some m-BINS, highlighted with yellow circles and only one aggregation, identified by a white circle. Figure 9D2 shows a possible crack initiation in the host matrix marked with a yellow circle; this can confirm the strong interface between m-BINS and the matrix. It is noteworthy to mention that in most polymer composites the crack origins are usually at the interface between filler and matrix.

4.5 | Chemical resistance

The chemical resistance and liquid penetration measurements are needed to assess polymers in some applications, such as marine industry and coating. Therefore, samples were cut and weighed. Then, they were soaked in various liquids, namely, deionized water, 5 wt% H_2SO_4 and 5 wt% NaOH solutions for a duration of 7 days. The samples were weighed every day; the weight gain rate was calculated following the equation: mass gain $(\%) = (W_b - W_a) \times 100/W_b$, where W_b and W_a are the weights of the sample before and after soaking. Neat epoxy and its 0.75-vol% nanocomposite were chosen as representative samples for chemical resistance tests. Figure 10A–C represents mass gain of neat epoxy and its nanocomposites in water, H_2SO_4, and NaOH solutions. It is evident that liquid intakes are faster and paramount in the first 3 days, especially for neat epoxy. Then, the increments in the intakes slow down and almost saturated by the end of the seventh day. Acidic environment is harsh for polymers; therefore, it is noticed that neat epoxy absorbed and gained larger mass in H_2SO_4 solution in comparison with water and alkaline solution (NaOH); neat epoxy gained mass of 2.25% in H_2SO_4 solution; and 1.75% in both water and NaOH solutions after 7 days immersion.

Upon adding plate-like structure fillers, such as BINS, epoxy matrix intakes are much lower than neat epoxy as shown in Figure 10A–C. The effect of modification on the chemical resistance of epoxy nanocomposites is highly noticeable. Epoxy/m-BINS nanocomposite reaches saturation in absorption for all three liquids by the fourth day, and almost ceases to absorb any of the liquids over the subsequent 3 days. Also, the amount of gained mass is marginal in comparison to neat epoxy or pristine BINS nanocomposite; for example, after 7 days in water,

epoxy/m-BINS absorbed 0.25% mass in comparison with 1.75% for neat epoxy and 1.1% for pristine BINS-system.

The chemical resistance behavior of neat epoxy and its nanocomposites can be explained as follows:

- Neat epoxy consists of 3D crosslinked molecules. Although those molecules are entangled, they still have spaces for liquids to penetrate and gain mass. This is schematically presented in Figure 10D; the liquid paths within the matrix are many and direct.
- When pristine BINS added into epoxy matrix, they work as physical barrier for the liquid attack. In addition, the fillers work as solid substances filling the voids within the matrix so that the matrix does not have space to intake much liquid. Therefore, the matrix absorbs less liquid. However, pristine BINS were not undergone ball milling which means large overlap distance and high chance of clustering due to van der Waal forces. This will allow some liquid to get into the matrix though it is less than the neat polymer as shown in Figure 10E.

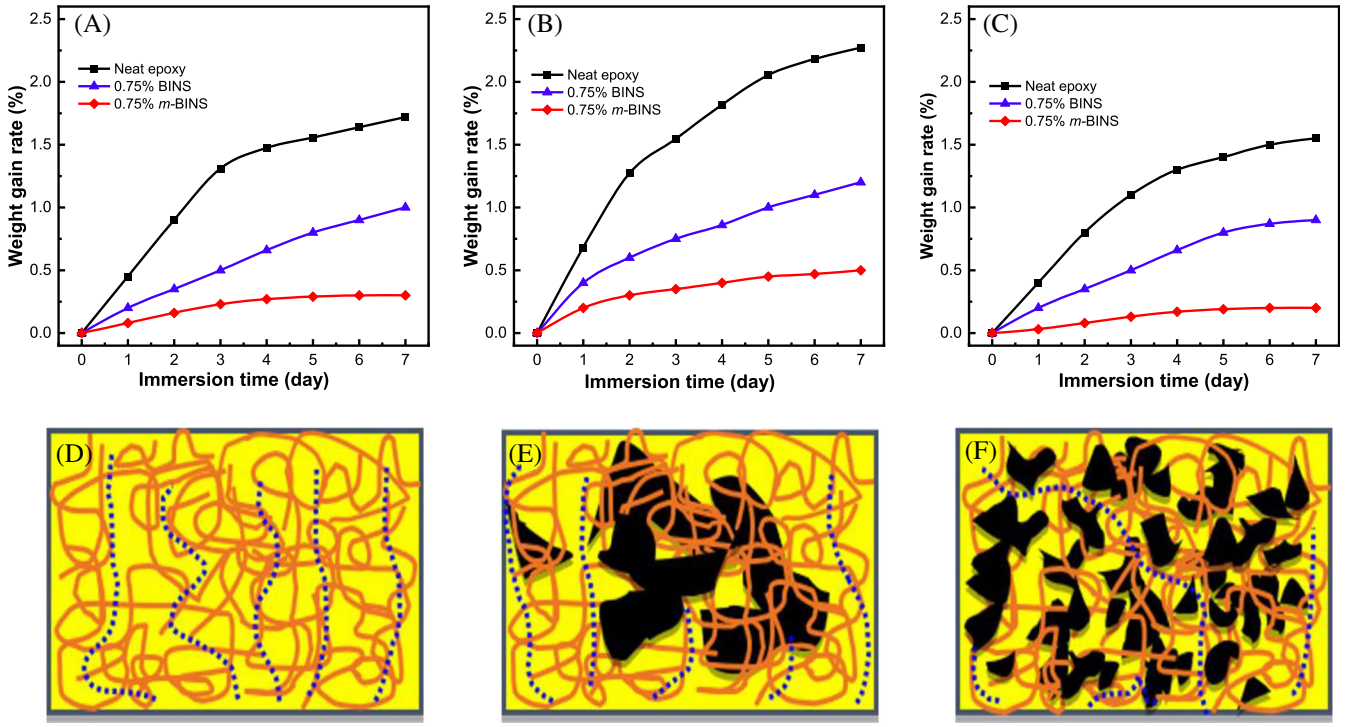

FIGURE 10 Chemical resistance of neat epoxy and its nanocomposites: (A) deionized water; (B) 5 wt% H_2SO_4; and (C) 5 wt% NaOH. Schematic of liquid penetration into epoxy nanocomposites: (D) neat epoxy; (E) epoxy/BINS; and (F) epoxy/m-BINS.

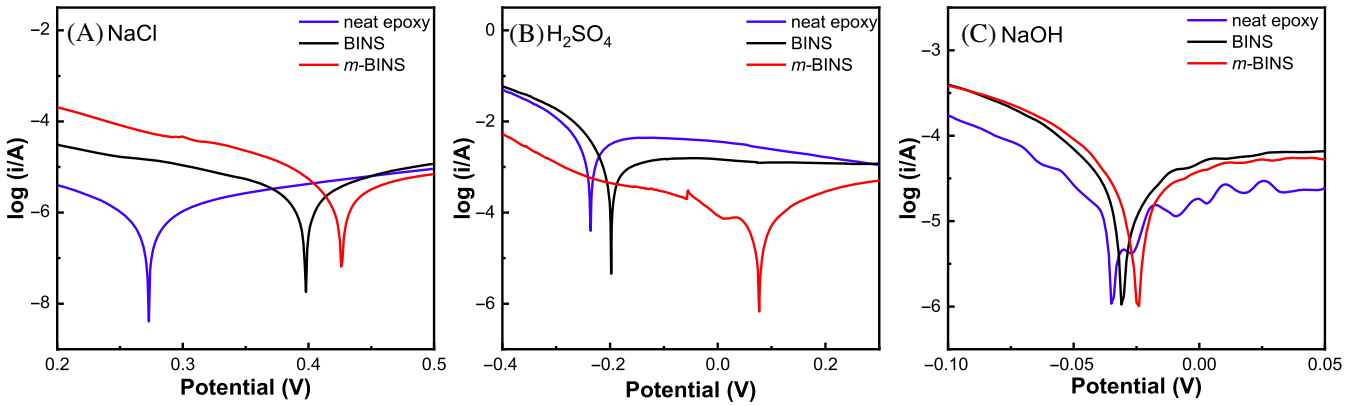

FIGURE 11 Tafel polarization curves of neat epoxy and its nanocomposites: (A) 5 wt% NaCl; (B) 5 wt% H_2SO_4; and (C) 5 wt% NaOH. BINS, bismuthene nanosheets; m-BINS, modified BINS.

- Upon modifying BINS via ball-milling process, they were broken into smaller sheets and wrapped with D-400 surfactant. This helps in uniformly distributing m-BINS within the matrix. In addition of being physical barrier, the well-distributed m-BINS create a more intricate pathway for water absorption in the epoxy as shown in Figure 10F; thereby enhancing the material's resistance to liquid penetration. Improving the compatibility and interaction between the filler and the matrix can enhance the adhesion of the interface region. Consequently, it prevents the matrix expansion caused by chain redirection and reduces the occurrence of structural instability, ultimately limiting the material's ability to absorb additional solvents.

4.6 | Electrochemical tests

Electrochemical testing is widely used to analyze the corrosion resistance of materials. In this study, three typical examples were tested: neat epoxy, 0.75 vol% epoxy/BINS nanocomposite, and 0.75 vol% epoxy/m-BINS nanocomposite. The materials were subjected to simulated environmental corrosion using 5 wt% NaCl, 5 wt% H_2SO_4, and 5 wt% NaOH, respectively. The Tafel polarization curves of the three materials are presented in Figure 11.

In the salt solution, the breakdown voltage of 0.75 vol % epoxy/BINS nanocomposite was significantly higher than that of pure epoxy, and the breakdown voltage of 0.75 vol% epoxy/m-BINS nanocomposite was further improved. While 0.75 vol% epoxy/BINS nanocomposite exhibited a slight increase in breakdown voltage in salt solutions, 0.75 vol% epoxy/m-BINS nanocomposite demonstrated a significant increase. This indicates that 0.75 vol% epoxy/m-BINS nanocomposite exhibits superior resistance to acid corrosion, possibly due to the improved dispersion and stronger interface of m-BINS in the epoxy matrix. These nanofillers enhance the barrier properties of the composite, reducing the diffusion of corrosive agents into the material.

Both composites showed a gradual increase in breakdown voltage in alkaline solutions. The increased breakdown voltage of the materials indicates that both composites possess enhanced corrosion resistance, with 0.75 vol% epoxy/m-BINS nanocomposite demonstrating the highest corrosion resistance among all three environments. Based on the findings of this study, we have identified several areas for future research: exploring different nanofillers, long-term performance and durability, application-specific studies, advanced characterization techniques, and scaling up the synthesis process.

5 | CONCLUSIONS

This study demonstrated the successful synthesis and chemical modification of BINS using mechanochemical methods. The addition of m-BINS into epoxy matrix resulted in significant improvements in mechanical properties, thermal stability, and chemical resistance. For instance, at 0.75 vol%, the Young's modulus and impact strength of epoxy increased by 30% and 89%, respectively, compared with pristine BINS, which showed increments of only 10% and 55.7%. The FE simulations for high-speed impact loading showed a substantial strength gain with the addition of m-BINS. Furthermore, the epoxy/m-BINS nanocomposite exhibited exceptional chemical resistance, with significantly lower liquid intake rates compared with neat epoxy and epoxy/BINS nanocomposites. These results underscore the importance of interface and dispersion in enhancing the mechanical and chemical properties of polymer nanocomposites. The findings of this study provide a scalable method for synthesizing and modifying BINS and offer insights into developing functional polymer nanocomposites for various industrial applications.

ACKNOWLEDGMENTS

Sensen Han would like to thank Shiyanjia Lab (www.shiyanjia.com) for the AFM testing. This work was financially supported by the National Natural Science Foundation of China (52173077 & 51973123), the Liaoning Provincial Department of Education Series Project, Australia (LJKZ0187), the Natural Science Foundation of Liaoning Province (2023-MS-239), and the Liaoning BaiQianWan Talents Program, China (2021921081); Nazarbayev University, Collaborative Research Grant ID 20122022CRP1613.

DATA AVAILABILITY STATEMENT

The data that support the findings of this study are available from the corresponding author upon reasonable request.

ORCID

Qingshi Meng https://orcid.org/0000-0002-8187-7028
Sherif Araby https://orcid.org/0000-0001-6807-7926

REFERENCES

1. Han S, Zhang X, Wang P, et al. Mechanically robust, highly sensitive and superior cycling performance nanocomposite strain sensors using 3-nm thick graphene platelets. *Polym Test*. 2021;98:107178. doi:10.1016/j.polymertesting.2021.107178
2. Meng Q, Zhao J, Zhou Z, et al. Damage monitoring of aircraft structural components based on large-area flexible graphene strain sensors. *Sens Actuators A*. 2024;369:115092. doi:10.1016/j.sna.2024.115092

3. Song P, Liu B, Qiu H, Shi X, Cao D, Gu J. MXenes for polymer matrix electromagnetic interference shielding composites: a review. *Compos Commun*. 2021;24:100653. doi:10.1016/j.coco.2021.100653
4. Zhang J, Wang X, Hang G, et al. Polypyrrole in-situ polymerized MXene/TPU fiber electrode for flexible supercapacitors. *Compos Commun*. 2024;45:101817. doi:10.1016/j.coco.2024.101817
5. Fang H, Bai S-L, Wong CP. "White graphene"—hexagonal boron nitride based polymeric composites and their application in thermal management. *Compos Commun*. 2016;2:19-24. doi:10.1016/j.coco.2016.10.002
6. Han S, Meng Q, Qiu Z, et al. Mechanical, toughness and thermal properties of 2D material-reinforced epoxy composites. *Polymer*. 2019;184:121884. doi:10.1016/j.polymer.2019.121884
7. Wang S, Cai R, Xue H, et al. Development of high thermally conductive and electrically insulated epoxy nanocomposites with high mechanical performance. *Polym Compos*. 2021;42:4217-4226. doi:10.1002/pc.26140
8. Han S, Yang F, Li Q, Sui G, Kalimuldina G, Araby S. Synergetic effect of alpha-ZrP nanosheets and nitrogen-based flame retardants on thermoplastic polyurethane. *ACS Appl Mater Interfaces*. 2023;15(13):17054-17069. doi:10.1021/acsami.2c20482
9. Han S, Li Q, Ma N, Liu D, Sui G, Araby S. Supramolecular-wrapped α-zirconium phosphate nanohybrid for fire safety and reduced toxic emissions of thermoplastic polyurethane. *ACS Appl Polym Mater*. 2024;6:1376-1388. doi:10.1021/acsapm.3c02481
10. Han S, Li S, Liu D, et al. Enhancing flame retardancy, anti-impact, and corrosive resistance of TPU nanocomposites using surface decoration of α-ZrP. *Polym Compos*. 2024;45:9209-9223. doi:10.1002/pc.28404
11. Wang T, Meng Q, Araby S, et al. Non-oxidized graphene/metal composites by laser deposition additive manufacturing. *J Alloys Compd*. 2021;882:160724. doi:10.1016/j.jallcom.2021.160724
12. Li P, Cai R, Yang G, et al. Mechanically strong, stiff, and yet ductile $AlSi_7Mg$/graphene composites by laser metal deposition additive manufacturing. *Mater Sci Eng A*. 2021;823:141749. doi:10.1016/j.msea.2021.141749
13. Meng Q, Song X, Han S, et al. Mechanical and functional properties of polyamide/graphene nanocomposite prepared by chemicals free-approach and selective laser sintering. *Compos Commun*. 2022;36:101396. doi:10.1016/j.coco.2022.101396
14. Verma A, Baurai K, Sanjay MR, Siengchin S. Mechanical, microstructural, and thermal characterization insights of pyrolyzed carbon black from waste tires reinforced epoxy nanocomposites for coating application. *Polym Compos*. 2020;41(1):338-349. doi:10.1002/pc.25373
15. Verma A, Negi P, Singh VK. Experimental analysis on carbon residuum transformed epoxy resin: chicken feather fiber hybrid composite. *Polym Compos*. 2019;40(7):2690-2699. doi:10.1002/pc.25067
16. Marichelvam MK, Manimaran P, Verma A, et al. A novel palm sheath and sugarcane bagasse fiber based hybrid composites for automotive applications: an experimental approach. *Polym Compos*. 2021;42(1):512-521. doi:10.1002/pc.25843
17. Bharath KN, Madhu P, Gowda TGY, Verma A, Sanjay MR, Siengchin S. A novel approach for development of printed circuit board from biofiber based composites. *Polym Compos*. 2020;41(11):4550-4558. doi:10.1002/pc.25732
18. Meng Q, Zhang X, Li S, et al. Bismuth oxyiodide nanorods towards improvements in fire safety and mechanical properties of natural rubber. *Polym Degrad Stab*. 2024;225:225. doi:10.1016/j.polymdegradstab.2024.110770
19. Meng Q, Yang Y, Han S, Meng F, Liu T. Preparation of high-performance bismuthene thermoelectric composites doped with graphene using UV-curing 3D printing technology. *Polym Compos*. 2024;45:8176-8186. doi:10.1002/pc.28332
20. Liu Y, Benter S, Ong CS, et al. A 2D bismuth-induced honeycomb surface structure on GaAs(111). *ACS Nano*. 2023;17(5):5047-5058. doi:10.1021/acsnano.2c12863
21. Mohan R. Green bismuth. *Nat Chem*. 2010;2(4):336. doi:10.1038/nchem.609
22. Yi M, Shen Z. Kitchen blender for producing high-quality few-layer graphene. *Carbon*. 2014;78:622-626. doi:10.1016/j.carbon.2014.07.035
23. Han S, Li S, Zhang X, et al. Enhancing the protective performance of anti-impact, corrosion resistant and flame retardant polyurea coatings using bio-based supramolecular decorated montmorillonite. *Construct Build Mater*. 2024;435:136721. doi:10.1016/j.conbuildmat.2024.136721
24. Han S, Yang F, Li Q, et al. Tackling smoke toxicity and fire hazards of thermoplastic polyurethane by mechanochemical combination of Cu_2O nanoparticles and zirconium phosphate nanosheets. *Polym Degrad Stab*. 2023;212:110350. doi:10.1016/j.polymdegradstab.2023.110350
25. Thirumal V, Yuvakkumar R, Kumar PS, et al. Efficient photocatalytic degradation of hazardous pollutants by homemade kitchen blender novel technique via 2D-material of few-layer MXene nanosheets. *Chemosphere*. 2021;281:130984. doi:10.1016/j.chemosphere.2021.130984
26. Han S, Yang F, Meng Q, et al. Using renewable phosphate to decorate graphene nanoplatelets for flame-retarding, mechanically resilient epoxy nanocomposites. *Prog Org Coat*. 2023;182:107658. doi:10.1016/j.porgcoat.2023.107658
27. Musteață AE, Pirvu C, Deleanu L, Georgescu C. Simulation of Charpy test for different impact velocities. *IOP Conf Ser Mater Sci Eng*. 2019;514(1):012011. doi:10.1088/1757-899X/514/1/012011
28. Kadioglu F, Demiral M, El Zaroug M. Effects of overlap length on the strength of bolted, bonded and hybrid single lap joints with different adherend materials and thicknesses. *J Adhes Sci Technol*. 2019;33(20):2191-2206. doi:10.1080/01694243.2019.1623966
29. Demiral M, Tanabi H, Sabuncuoglu B. Experimental and numerical investigation of transverse shear behavior of glass-fibre composites with embedded vascular channel. *Compos Struct*. 2020;252:112697. doi:10.1016/j.compstruct.2020.112697
30. Jung H, Choi HK, Lee H-S, Kim Y, Yu J. High strain rate effects on mechanical properties of inductively coupled plasma treated carbon nanotube reinforced epoxy composites. *Compos B Eng*. 2018;154:209-215. doi:10.1016/j.compositesb.2018.08.015
31. Li J, Yang F, Liu D, Han S, Li J, Sui G. Graphene composite paper synergized with micro/nanocellulose-fiber and silk fibroin for flexible strain sensor. *Int J Biol Macromol*. 2023;240:124439. doi:10.1016/j.ijbiomac.2023.124439
32. Meng Q, Feng Y, Han S, et al. Developing functional epoxy/graphene composites using facile in-situ mechanochemical approach. *J Appl Polym Sci*. 2023;140:e53681. doi:10.1002/app.53681

33. Zaman I, Kuan H-C, Meng Q, et al. A facile approach to chemically modified graphene and its polymer nanocomposites. *Adv Funct Mater*. 2012;22(13):2735-2743. doi:10.1002/adfm.201103041
34. Naeem M, Kuan H-C, Michelmore A, et al. Epoxy/graphene nanocomposites prepared by in-situ microwaving. *Carbon*. 2021;177:271-281. doi:10.1016/j.carbon.2021.02.059
35. Han S, Wang P, Zhou Y, Meng Q, Aakyiir M, Ma J. Flexible, mechanically robust, multifunctional and sustainable cellulose/graphene nanocomposite films for wearable human-motion monitoring. *Compos Sci Technol*. 2022;230:109451. doi:10.1016/j.compscitech.2022.109451
36. Zhang S, Guo S, Chen Z, et al. Recent progress in 2D group-VA semiconductors: from theory to experiment. *Chem Soc Rev*. 2018;47(3):982-1021. doi:10.1039/C7CS00125H
37. Han S, Meng Q, Araby S, Liu T, Demiral M. Mechanical and electrical properties of graphene and carbon nanotube reinforced epoxy adhesives: experimental and numerical analysis. *Compos Part A: Appl Sci Manuf*. 2019;120:116-126. doi:10.1016/j.compositesa.2019.02.027

How to cite this article: Meng Q, Li S, Guo F, et al. A facile approach for enhancing mechanical resilience, and corrosion protection in epoxy coatings using bismuthene nanosheets. *Polym Compos*. 2024;45(16):14966-14981. doi:10.1002/pc.28814